JOURNAL OF MATERIALS SCIENCE 25 (1990) 45–53

Effect of phase transformations on the creep rupture properties of two type 316 weld metals

B. A. SENIOR
Research Division, Central Electricity Generating Board, Central Electricity Research Laboratories, Kelvin Avenue, Leatherhead, Surrey KT22 7SE, UK

Many of the factors which give rise to the low and variable creep rupture properties of type 316 weld metals are not yet fully understood. In the present study two weldments fabricated using the same welding parameters, but with compositional differences which give rise to different weight fractions of sigma phase and $M_{23}C_6$ carbides have been examined after creep testing. It was found that lower creep rupture strength and ductility was associated with higher weight fractions of sigma phase, which give rise to a higher number density of cavities at low deformation levels and facilitate crack propagation along sigma–austenite interfaces. The observed microstructural differences have been explained with reference to the predictions which can be made using thermodynamic analysis.

1. Introduction

AISI type 316 austenitic stainless steel has been widely used in both conventional and nuclear power plant for high temperature components, and is the preferred material for several components in the fast reactor programme. The type 316 steel has a good creep rupture strength, but several studies (e.g. [1]) have shown that considerable variation in creep ductility exists. A tye 316 material with improved properties, designated 316L(N), has been developed for fast reactor applications [2], and may find considerable application in both conventional and nuclear power plants in the future.

Recent surveys have, however, shown that the variable creep ductility observed in type 316 material is also exhibited by type 316 (19Cr–12Ni–3Mo) weldments and the leaner 17Cr–8Ni–2Mo weldments [3]. The development of electrodes which result in weldments with good creep rupture properties has consequently been identified as a necessary prerequisite to the ultilization of type 316L(N) material.

The present study forms part of a wider investigation into the interrelationships between the long-term creep properties and microstructure of type 316 weldments. In the present study the effect of high levels of sigma phase on creep rupture strength and ductility have been examined using weldments fabricated using two electrode types. Weld A is a type 19Cr–12Ni–3Mo and weld B a type 17Cr–8Ni–2Mo, electrode, both with a rutile coating.

The effects of sigma phase on toughness have been known for some time [4], a higher sigma phase content being associated with low toughness. The effects of sigma phase precipitation on creep rupture properties have not been examined in detail, but recent observations relating to wrought 316 material have shown that poor creep rupture properties are associated with high sigma phase contents. Thomas [6] and Farrar [7, 8] have demonstrated that the short-term creep properties of type 316 weld metals are strongly influenced by the nature and extent of ferrite transformation products.

2. Experimental procedures

2.1. Materials

Type 316 plate-to-plate butt welds were deposited using the manual metal arc process along a 76 cm single U groove. The bulk chemical compositions of the resultant weldments are given in Table I; as noted previously, both of the electrode types had a rutile coating.

2.2. Creep rupture testing

Creep rupture testing at 600° C was performed by the Electrical Research Association, and two specimen orientations, parallel (longitudinal) and perpendicular (cross-weld) to the welding direction were tested.

2.3. Microstructural characterization

Following creep rupture testing samples from the grip and gauge length of specimens were prepared for optical examination using standard metallographic techniques. When necessary, specimens were etched electrolytically in a 10% HCl–methanol solution.

2.3.1. Ferrite measurement

The residual ferrite level in all samples was measured directly using a Ferritscope, calibrated against a series of known standards. Since the ferrite content can vary considerably in a multi-pass weldment [9], the mean of six readings in mutually perpendicular directions was taken.

2.3.2. Inclusion content

The inclusion content of the welds was assessed quantitatively using an image analysis system. Polished sections from the grip of pre-crept specimens were

0022–2461/90 $03.00 + .12

TABLE I Bulk chemical compositions of the weld materials used in this investigation

Weld metal	Weight %													
	C	Cr	Co	Cu	Mn	Mo	Ni	Nb	P	Si	S	V	N	B
A	0.033	18.1	0.03	0.05	0.9	2.8	11.3	< 0.1	0.016	0.45	0.01	0.04	0.046	< 0.0001
B	0.069	17.3	0.03	0.06	1.89	2.00	9.4	< 0.1	0.017	0.40	0.005	0.076	0.037	0.0003

examined at a magnification of × 500, using random fields and traversing several weld beads.

The composition of inclusions was determined using energy dispersive (EDX) spectroscopic analysis of inclusions extracted on to carbon replicas and examined in a Hitachi H700H transmission electron microscope (TEM) with scanning (STEM) capability.

2.3.3. Precipitate analysis

2.3.3.1. Bulk X-ray analysis. Samples were taken for X-ray analysis using the technique developed by Chung [10] and applied to austenitic steels by Lai and Galbraith [11]. In order to minimize errors arising from the dissolution of sigma phase [12], the analysis was performed on precipitates extracted under controlled conditions for 6 h at a current density of 0.04 A cm^{-2}.

2.3.3.2. STEM–EDX analysis. Detailed analysis of the precipitates formed during creep testing was performed using carbon extraction replicas, prepared from polished and lightly etched surfaces. Extracted particles were analysed using EDX analysis in the Hitachi H700H (STEM mode) at an accelerating voltage of 200 kV and magnifications between × 10 000 and × 100 000. The analysis conditions gave count rates in the range 800 to 3500 c.p.s. The precipitate types corresponding to EDX spectra obtained were established by comparing the spectra with calibrated spectra for type 316 material [13, 14].

2.4. Post test metallography

In order to establish the mode of failure, the fracture surfaces of all specimens were examined in a Hitachi S800 high resolution scanning electron microscope (SEM). Samples taken from the gauge length of precrept specimens were examined both optically and in the SEM for evidence of cavitation and cracking.

3. Experimental results

3.1. Creep rupture testing

Fig. 1 shows creep rupture results from the type A and type B weld metals. Creep ductility results are shown in Fig. 2. It is evident from these data that the creep rupture stength of the type A weld metal is significantly lower than that of the type B weld metal, and that this is associated with a lower creep ductility at a given time in all tests. It is important to note that the long term creep ductility of weld metal A is very low (~ 1%).

3.2. Microstructural characterization

3.2.1. General microstructure

Optical micrographs typical of the observed microstructures are shown in Fig. 3. The prior ferrite morphology in all samples examined was similar, with a skeletal morphology in all regions except close to the fusion zone, where some decomposition to a granular morphology had occurred.

The skeletal morphology is indicative of a primary ferritic solidification mode, with some austenite formation from the last of the melt to solidify. Kujanpaa *et al.* [15] have shown that this mode of solidification is associated with $(Cr–Ni)_{eq}$ values between 1.48 and 1.95 (Schaeffler, [16] equivalents), and the present results are consistent with this. Examination of several specimens confirmed that the prior ferrite network was not continuous in weld B, but some regions of weld A contained a largely continuous ferrite network, consistent with the higher ferrite content of this weldment. During creep testing, these regions became discontinuous as ferrite decomposition occurred.

The inclusion content of the two weldments examined is summarized in Table II. The size, morphology and distribution of inclusions in the weldments were similar. EDX analysis of the inclusions present suggested that these were predominantly manganese silicates.

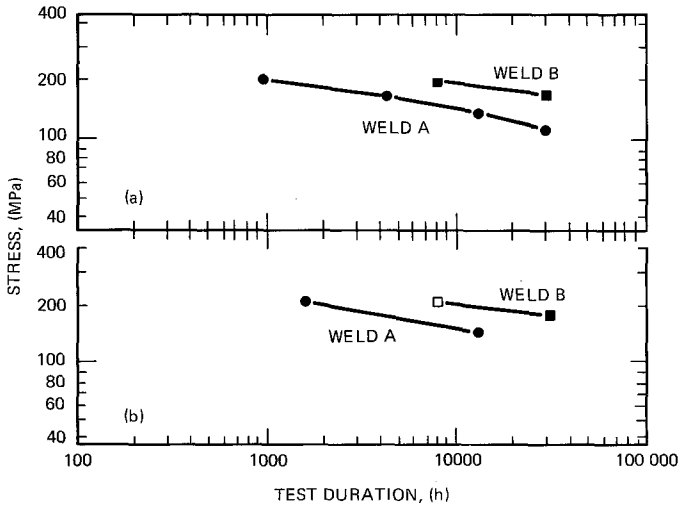

Figure 1 Creep rupture curves for the weldments used in this investigation. Open symbol denotes fracture outside the weld metal. (a) Longitudinal, (b) cross weld.

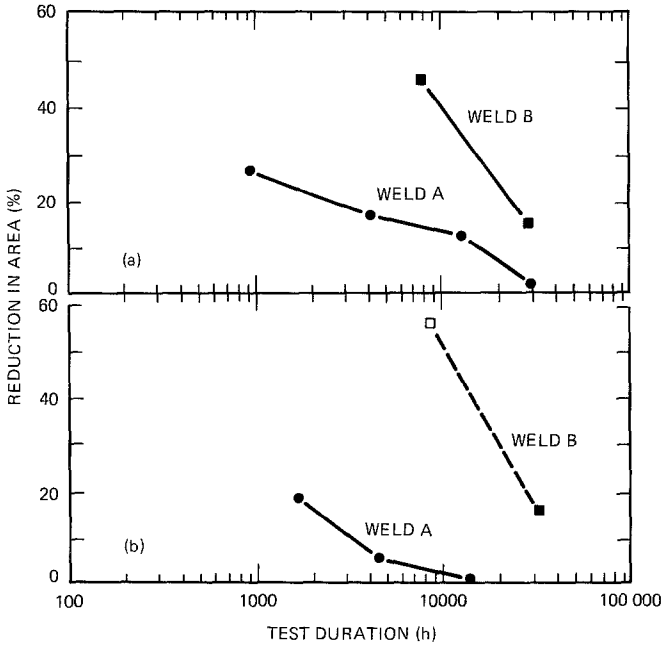

Figure 2 Creep ductility data for the two weldments examined. Open symbol denotes fracture outside the weld metal. (a) Longitudinal, (b) cross weld.

3.2.2. Ferrite content

The measured ferrite content of samples taken from the gauge length and grip are shown in Table III, together with measured values for the weldments before creep testing. It is evident from the data shown in Table III that the kinetics of ferrite decomposition are significantly higher in weld A. Comparison of the value for the B2 grip sample (aged 28 293 h at 600° C) with that for the A5 grip sample (aged 28 716 h at 600° C) shows ~98% transformation in the latter, but only ~76% in the B2 grip sample. Similar results are obtained if shorter term tests are compared.

Comparison of the results obtained from the grip (aged) and gauge length (creep tested) of specimens shows more extensive ferrite transformation has occurred in the gauge length in all specimens. As noted previously [12], this is almost certainly due to the rapid diffusion rates associated with high dislocation densities in the deforming material, which also leads to a greater scatter in some of the results from deformed material (Table III).

3.2.3. Precipitate analysis

3.2.3.1. Bulk X-ray analysis. The results from X-ray analysis of bulk extracted precipitates are summarized in Table IV. Only $M_{23}C_6$ and sigma phase were detected in the samples examined using this technique.

It is evident from the results given in Table IV that the weight fraction of sigma phase in all weld A specimens exceeds that present in the weld B samples, and that the weight fraction of $M_{23}C_6$ in the weld A specimens is generally lower.

TABLE II Summary of the inclusion content of the weldments

Material	Mean diameter (μm) (eq.)*	Number density (m^{-2})	Mean aspect ratio
A	1.53	2.4×10^{10}	1.37
B	1.42	3.3×10^{10}	1.30

*(eq.) denotes equivalent diameter assuming a sphere with the same area as the particle observed.

The scatter in results is, however, significant and precludes a more detailed assessment of the data.

3.2.3.2. STEM-EDX analysis. The precipitate phases observed in the gauge length of all specimens are summarized in Table V. Large, blocky sigma phase particles were observed in all samples, generally following the prior ferrite morphology (Fig. 4a). Examples of $M_{23}C_6$ precipitation at prior ferrite sites were also noted in all specimens and, in B1 and B2 (which has a higher carbon content) the $M_{23}C_6$ frequently exhibited a morphology consistent with complete replacement of ferrite with $M_{23}C_6$ and austenite (Fig. 4b). Laves' type Fe_2Mo phase was observed in all samples, generally associated with prior ferrite transformation products. The volume fraction of all precipitates was observed to increase with greater test duration, the highest density and largest precipitates being present in B2 and A5.

Chi phase was also observed at prior ferrite sites, in samples from B2, B4 and B5. The size and morphol-

TABLE III Measured ferrite content of the samples examined. The standard deviations of the mean values are also shown

Weld metal	Sample	Test duration at 600° C, (h)	Location	% Ferrite
A	As-welded		–	8.2
	A1	914	Grip	2.50 ± 0.08
			Gauge length	1.25 ± 0.25
	A2	4 163	Grip	1.10 ± 0.07
			Gauge length	0.89 ± 0.08
	A4	12 590	Grip	0.37 ± 0.03
			Gauge length	0.25 ± 0.04
	A5	28 716	Grip	0.15 ± 0.03
			Gauge length	0.07 ± 0.03
B	As-welded		–	5.2
	B1	7 860	Grip	2.58 ± 0.07
			Gauge length	1.34 ± 0.07
	B2	28 293	Grip	1.24 ± 0.12
			Gauge length	1.12 ± 0.21

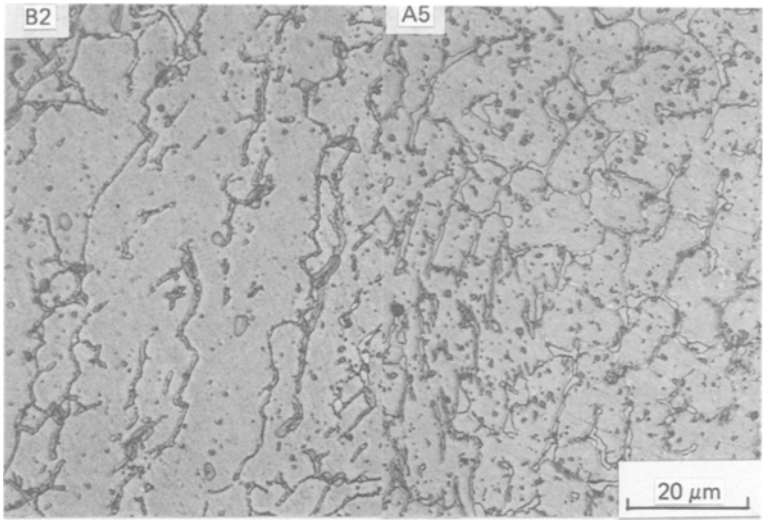

Figure 3 Optical micrograph showing the prior ferrite morphology in specimens B2 and A5.

ogy of this phase were similar to those of $M_{23}C_6$ particles, and it was noted that chi was more extensively present in A2 than in the longer term test materials A4 and A5. This result suggests that the molybdenum-rich chi phase may be less thermodynamically stable at 600° C than the intermetallic Laves' type Fe_2Mo phase.

In the interferritic regions, fine dispersions of acicular and spheroidal Fe_2Mo and generally spheroidal or ellipsoidal $M_{23}C_6$ were observed. Small amounts of sigma or chi were noted at interferritic sites in all samples (sigma) and A2–A5 (chi), respectively. Other precipitates such as VC and NbC were not detected in any of the samples examined.

3.3. Post test metallography

3.3.1. Specimen sections

Optical examination of polished sections revealed more extensive cavitation in the gauge length of samples from weld A, although cavitation and some cracking was observed in samples from both of the weldments. Fig. 5 shows examples of cracking in the gauge length of A1, close to the fracture surface.

Examination of lightly etched sections in the SEM confirmed that the major cavity nucleation sites were sigma and $M_{23}C_6$ particles at prior ferrite sites, although cavitation at inclusions and other matrix particles was also observed. Fig. 6 shows examples of cavitation at sigma and $M_{23}C_6$ in sectioned specimens. Some examples of sigma phase cracking were noted. Very few sigma phase particles did not have cavities formed at the interface or by particle cracking, but several examples of $M_{23}C_6$ without cavities on the carbide–austenite interface were observed, more frequently on sections from weld A specimens.

3.3.2. Fractography

The fracture surfaces of all specimens were similar, and typical features are shown in Fig. 7. Detailed examination confirmed that the principal fracture

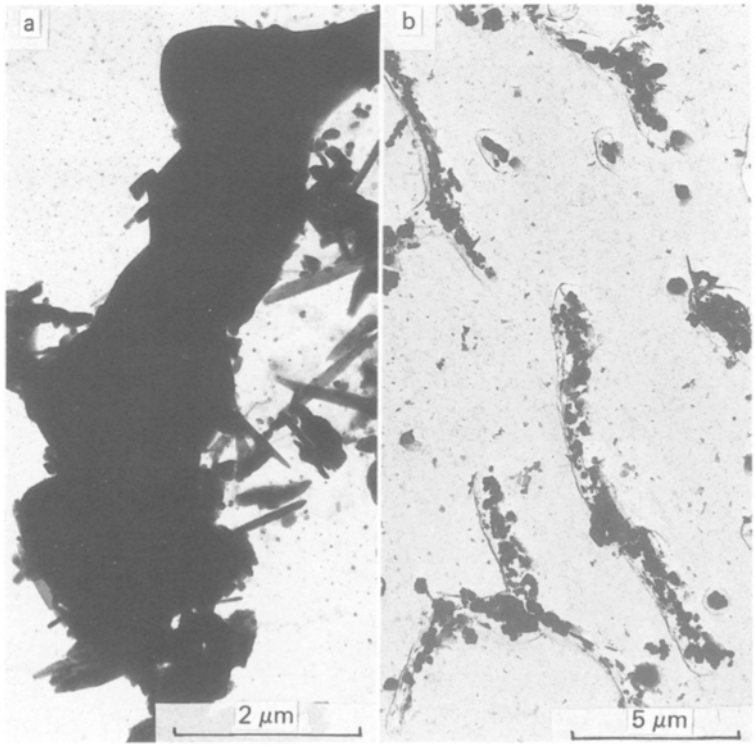

Figure 4 TEM micrographs of (a) sigma phase and (b) $M_{23}C_6$ in a prior ferrite morphology.

TABLE IV Bulk X-ray extraction analysis results

Weld metal	Sample	Location	wt %		
			$M_{23}C_6$	Sigma	Other*
A	A1	Grip	$\leqslant 1.47$	~ 2	
		Gauge Length	$\leqslant 0.95$	~ 3.5	
	A2	Grip	$\leqslant 1.17$	2.15	1.16
		Gauge Length	$\leqslant 0.76$	3.42	0.04
	A4	Grip	0.49	3.49	0.51
		Gauge Length	0.38	4.94	
	A5	Grip	0.56	4.38	0.67
		Gauge Length	0.38	3.79	1.634
B	B1	Grip	$\leqslant 1.63$		
		Gauge Length	$\leqslant 1.95$		
	B2	Grip	1.31	0.37	0.86
		Gauge Length	1.35	1.95	

*The sum of $M_{23}C_6$ and sigma was frequently less than 100%, although peaks arising from other phases were not detected. In this case, the excess extract has been recorded in this column. High values in this column were associated with low absolute weights of extracted precipitate.

paths were prior ferrite transformation product–austenite interfaces, with ductile fracture in the last regions to separate.

4. Discussion

The results presented in Section 3 show that the creep rupture strength of the type A weld metal is lower than that of the type B weld metal, and that the lower creep rupture strength of weld A is associated with low ductility values. Full creep curves for the tests were not recorded, but the available data suggest that the creep rates of the two weldments may be significantly different. This difference may be attributable to the compositional differences in the two welds. Fine matrix precipitation was not observed, however, suggesting that variations in the levels of solid solution strengthening elements could be responsible. If this is so, the creep rupture curves (Fig. 1) indicate that weld A should be softer, a phenomenon which will result in improved creep ductility. The rupture ductilities of weld A specimens are, however, comparable or lower than the weld B specimens, suggesting that the rate of creep damage accumulation in weld A material is higher.

Several differences in the precipitation sequence and microstructure of the two weldments have been identified. If the interrelationships between microstructure and creep rupture properties are to be fully understood, however, the micromechanisms of failure must be clearly established. In addition, the factors giving rise to important microstructural differences must be identified if electrodes resulting in improved properties are to be effectively developed.

TABLE V Summary of precipitates identified on extraction replicas from the gauge length of creep specimens

Precipitate	Sample	
	Weld A	Weld B
$M_{23}C_6$	A1, A2, A4, A5	B1, B2
Sigma	A1, A2, A4, A5	B1, B2
Laves' Fe_2Mo	A1, A2, A4, A5	B1, B2
Chi	A2, A4, A5	

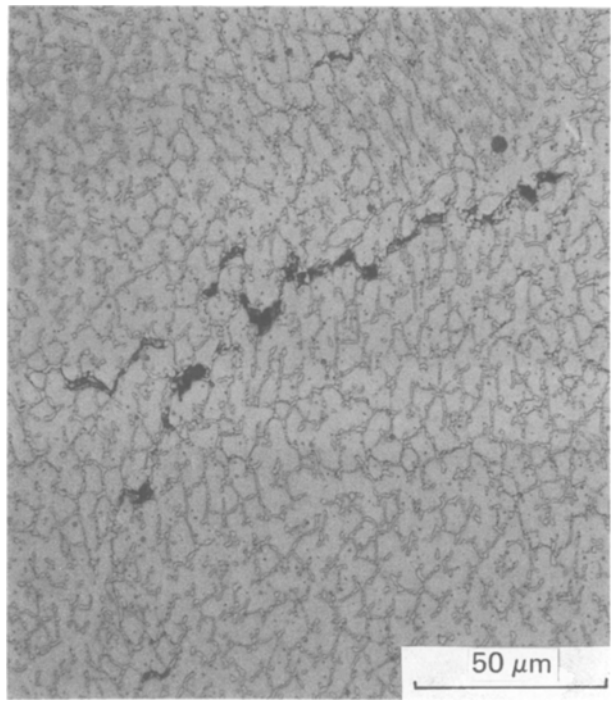

Figure 5 Cracks formed close to the fracture surface of specimen B1.

The mechanisms by which creep failure occurs in type 316 weld metals have been examined previously [6–8, 12], and may be summarized for ferrite-containing weld metals as follows.

(I) Cavity nucleation occurs, principally at prior ferrite transformation products, although inclusions may also provide important sites for cavity nucleation. Matrix strengthening may enhance nucleation as strain is accommodated locally to the precipitates.

(II) Nucleated cavities give rise to small cracks, which propagate along precipitate–austenite interfaces. A series of cracks with dimensions approximating to the extent of the continuous transformed ferrite network may be formed in this manner. If the network is continuous in large regions of the weld, failure of the specimen can occur at this stage.

(III) In the absence of a generally continuous prior ferrite network, the interfacial cracks arrest at the austenite matrix. Final rupture of the specimen then occurs as cracks propagate through the austenite. A high density of inclusions can facilitate propagation through the austenite as inclusion nucleated cavities coalesce with the advancing crack tip.

In the present study, cavities were observed principally at sigma–austenite and $M_{23}C_6$–austenite interfaces. Examples of sigma phase cracking and inclusion decohesion were also observed. The measured inclusion content of the two weldments was similar, and the interferritic precipitation levels were comparable in specimens from the two weldments tested for approximately equal times. Chi phase was observed in small quantities in several specimens from weld A, but few examples of cavitation at chi phase were noted.

The results summarized in Section 3.2. show that the rate of ferrite transformation and levels of sigma phase and $M_{23}C_6$ formed during ageing and creep testing are significantly different in the two weldments, however. Ferrite transformation in the weld A

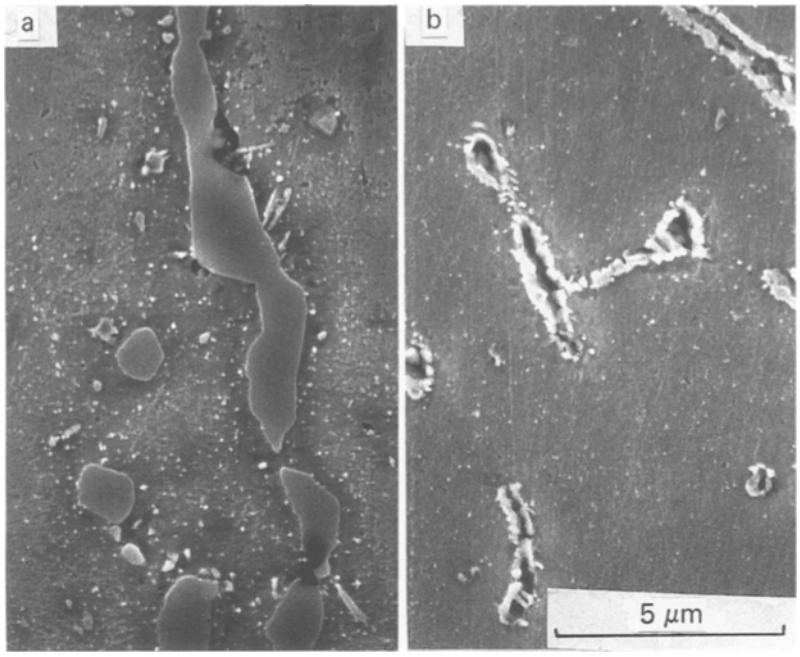

Figure 6 Examples of cavitation at (a) sigma phase and (b) $M_{23}C_6$ carbides in specimens B1 and A5, respectively.

specimens was more rapid, and these specimens contain a higher weight fraction of sigma phase and a lower weight fraction of $M_{23}C_6$. The results presented in Section 1 show that this precipitation is associated with consistently lower creep rupture strength and ductility.

If these results are considered in conjunction with the post test metallography and the failure mechanism outlined above, two possible inferences may be made.

(i) Cavity nucleation (stage I above) occurs more readily at sigma phase precipitates than at $M_{23}C_6$ carbides. The number density of cavities in weld metal A will, therefore, be higher at a given level of deformation than the number density in similarly deformed weld B specimens. The creep rupture life of weld metal A will consequently be lower as crack formation and propagation occur at lower deformation levels. This inference is supported by the observation that almost all of the sigma phase particles examined were cavitated, whilst $M_{23}C_6$ carbides in the same specimens were frequently uncavitated.

(ii) The presence of a higher proportion of total precipitate, largely at prior ferrite sites, in the weld A specimens would be expected to result in a higher number density of cavities at a given level of deformation, and more rapid crack propagation as the extent of the transformed ferrite network is more continuous. In short-term tests using weld A specimens regions in which a continuous ferrite network was present were noted, suggesting that stage (III) (above) was not required for failure in these specimens.

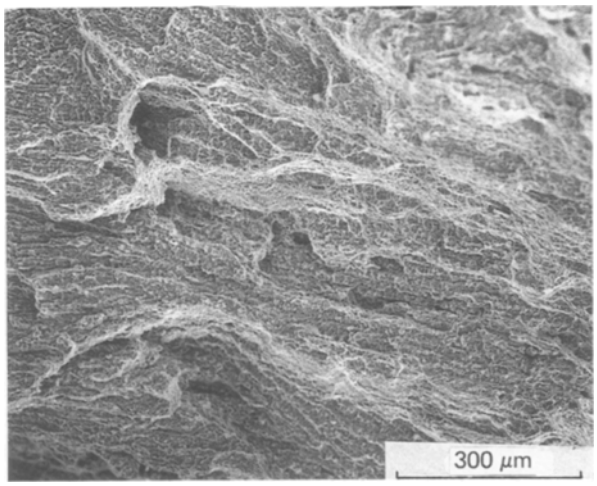

Figure 7 Fractography of specimen B2, showing features typical of all fracture surfaces.

The relative contribution of the two effects outlined above to the low ductility failures of the weld A specimens cannot be clarified by examination of the failed specimens only. The results obtained in the present study suggest, however, that both effects are significant.

It has been noted that ferrite transformation in the weld A specimens was more rapid, the weight fraction of sigma phase higher, and the weight fraction of $M_{23}C_6$ lower than in the weld B specimens. Farrar [7, 8] has suggested that these effects are interrelated, since a more widespread precipitation of $M_{23}C_6$ at ferrite–austenite interfaces will reduce and inhibit the formation of sigma phase, if the latter is assumed to be controlled by local chromium and molybdenum levels. These factors may be important in short-term tests, but during longer-term tests diffusion of chromium and molybdenum to the metastable ferrite occurs [17, 18] and chromium levels may be close to those of sigma phase. In short-term creep tests, therefore, the thermodynamic driving force for the formation of sigma phase is provided locally by metastable ferrite. Once formation of the ferrite is largely complete, however, the phases formed during decomposition of the ferrite must be stable with respect to the austenite matrix and an equilibrium based on the solubility of the phases in austenite will be established. In weld metal A more than 80% of the ferrite has transformed within 100 h at 600° C in the gauge length, with ~ 75% transformation in weld B in 7860 h.

In the longer-term tests to > 25 000 h it is consequently anticipated that thermodynamic equilibrium will be approached, particularly in the gauge length of specimens in which precipitation kinetics are accelerated.

The original ferrite content in such tests is less likely to determine the extent of precipitation than the solid solubility of the phases in austenite.

The solubility of $M_{23}C_6$ in type 316 material at 600° C can be calculated using the relationship obtained by Deighton [19] as 0.0004 wt % C. This value suggests that in the absence of other strong carbide forming elements, virtually all of the carbon will combine to form stable $M_{23}C_6$ carbides. If a formula of $Cr_{16}Fe_5Mo_2C_6$ is assumed [20], the weight fraction of $M_{23}C_6$ in the two weldments examined can be calculated as 1.32 wt % (weld B) and 0.63 wt % (weld A). These values are in general agreement with the results from bulk X-ray analysis (Table IV), the higher carbon content of weld B giving rise to a higher weight fraction. The data shown in Table IV also suggest that the maximum permissible weight fraction was precipitated after less than 5000 h in creep, although considerable scatter in the results obtained using bulk X-ray analysis is apparent. The rate of sigma formation was more sluggish than that of $M_{23}C_6$ precipitation in both of the welds examined.

The solid solubility of sigma phase is more difficult to assess quantitatively, since the occurrence of this phase is determined by a number of physical parameters including solute–solvent size difference and electronegativity [21]. In the design of nickel-based superalloys the so-called PHACOMP method has been widely used to predict the occurrence of sigma phase [22], but several limitations to a more general application of this method have become apparent, and a new approach based upon the d-orbital energy levels has recently been developed by Morinaga *et al.* [23, 24]. In this procedure the calculated energy level of the d-orbitals of the alloying transition metals (M_d) are used to obtain an average value, $\bar{M}_d$, which is sensitive to the electronegativity and atomic size of the alloying elements. This procedure has been successfully applied [24] to an Fe–Cr–Ni alloy and it has been shown that a higher $\bar{M}_d$ value indicates a stronger tendency for sigma formation and a higher volume fraction of sigma phase. A critical value, $\bar{M}_{dc}$, represents the $\gamma/(\gamma + \sigma)$ phase boundary and is temperature dependent.

It is of interest to note in this context that the effect of major transition elements on the sigma forming tendency is qualitatively similar to the effects implicit in the "nickel balance" approach used by Kihara *et al.* [5] and, to a lesser extent, the "chromium equivalent" approach suggested by Hull [25] as a means of assessing the tendency for embrittlement by sigma phase formation in austenitic steels.

The average value of M_d is defined by

$$\begin{aligned}\bar{M}_d = {} & 1.9(a_{Al} + a_{Si}) + 2.271a_{Ti} + 1.543a_V \\ & + 1.142a_{Cr} + 0.957a_{Mn} \\ & + 0.858a_{Fe} + 0.777a_{Co} + 0.717a_{Ni} \\ & + 0.615a_{Cu} + 2.117a_{Nb} + 1.55a_{Mo} \\ & + 3.020a_{Hf} + 2.224a_{Ta} + 1.655a_W \qquad (1)\end{aligned}$$

where a_M is the atomic fraction of M present in the steel.

Calculation of $\bar{M}_d$ for the two welds examined yields values of 0.9124 (weld B) and 0.9167 (weld A). For a 25%Cr–20%Ni austenitic steel, Ezaki *et al.* [24] have shown that a difference in $\bar{M}_d$ of 0.0043 may give rise to a difference in sigma phase volume fraction of 3 to 4%. A brief survey of published data is contained in Appendix and indicates that the critical $\bar{M}_d$ for sigma formation in type 316 material at 600 to 650° C is 0.906. The analysis, therefore, suggests that sigma phase will form in both of the weldments, but that the thermodynamic driving force for sigma formation, and the volume fraction of sigma phase, will be greater in weld metal A. These results are in general agreement with the experimental data obtained in the present study.

The effects of $M_{23}C_6$ precipitation on the $\bar{M}_d$ value are small. The formation of 1.32 wt % of $M_{23}C_6$ in the weld B results in a change in $\bar{M}_d$ of 0.0002. The precipitation of Laves' type Fe_2Mo and the presence of manganese silicate inclusions in both of the weldments will alter $\bar{M}_d$ by similar amounts for both weldments, and the precipitation of small amounts of chi phase in some of the weld A specimens will have little effect on the matrix composition. The high $\bar{M}_d$ of weld metal A relative to that of weld metal B will consequently be maintained.

The predictions made using the $\bar{M}_d$ approach are, therefore, consistent with the experimental data and provide a physical explanation of the more extensive sigma phase precipitation observed in weld A specimens.

5. Conclusions

On the basis of the results presented in this study it may be concluded that:

(i) The creep rupture mechanism in both of the weldments was cavity nucleation, principally at prior ferrite transformation products, followed by crack formation along precipitate–austenite interfaces and subsequent propagation through the austenite matrix.

(ii) Weld metal A has consistently lower creep rupture strength and ductility than weld metal B.

(iii) The rapid accumulation of creep damage in the weld A specimens relative to damage accumulation in the weld B is attributable to the high weight fractions of sigma phase formed in these specimens during creep testing. It can be inferred from the results obtained that a high density of sigma particles gives rise to a higher number density of cavities at low deformation levels, and also facilitates rapid crack propagation along sigma–austenite interfaces.

(iv) Initially high delta ferrite levels can give rise to a generally continuous crack propagation path as the delta ferrite and associated transformation products form a continuous network. During long-term testing, however, the network may become discontinuous as equilibrium between the sigma phase and austenite, rather than sigma phase and metastable ferrite, is established.

(v) The observed differences in $M_{23}C_6$ precipitation in the two weldments are in good agreement with predictions made using thermodynamic analysis.

(vi) The higher sigma levels observed in weld A

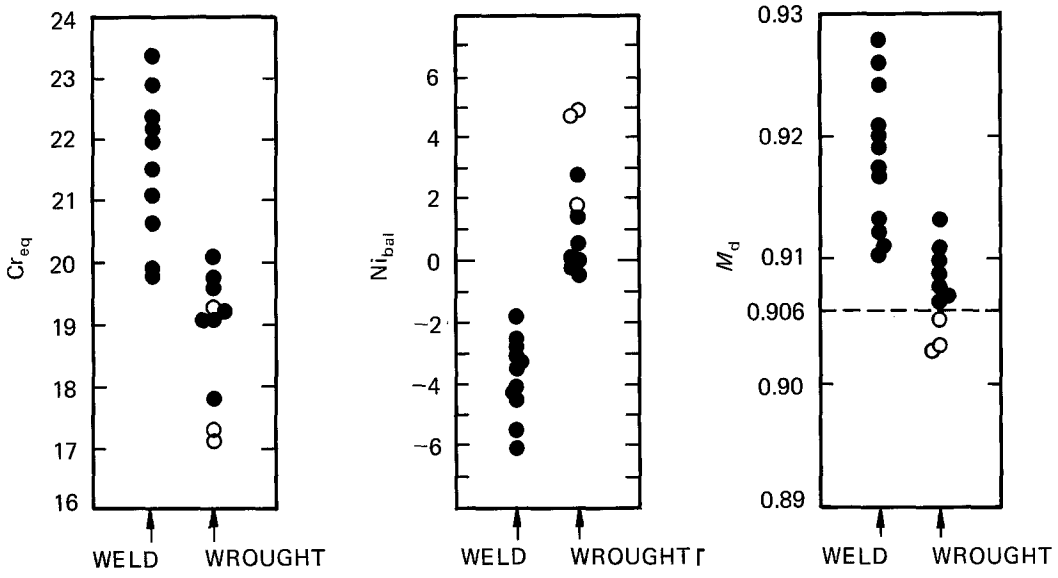

Figure A1 Occurrence of sigma phase in type 316 steel (wrought and weld), shown as a function of Cr_{eq}, Ni_{bal} and $\bar{M}_d$. Ageing or creep testing at 600 to 650° C. (●) Sigma detected, (○) sigma not detected (> 100 000 h ageing).

specimens after long-term creep testing may be explained by reference to the $\bar{M}_d$ approach developed by Morinaga *et al.* [23, 24] to describe the solid solubility of intermetallic phases in fcc metals.

Acknowldegements

The author would like to thank Mr A. Chowdhury for his assistance in specimen preparation, and Mr I. Pearce for performing the X-ray analysis of extracted precipitates.

This work was carried out at the Central Electricity Research Laboratories and is published by permission of the Central Electricity Generating Board. Creep rupture data and tested specimens were supplied by the Electrical Research Association.

Appendix: use of $\bar{M}_d$ to predict sigma formation in type 316 material

A survey of the available literature yields information relating to the occurrence, or otherwise, of sigma phase in type 316 wrought and weld material after long-term thermal ageing or creep testing at 600 to 650° C. Data from the studies of Kihara *et al.* [5], Inagaki *et al.* [26], Minami *et al.* [27], Spaeder and Brickner [28], Lai and Wickens [29], Senior [12] and the shorter-term data of Farrar and Thomas [17] are summarized in Fig. A1, plotted as a function of Cr_{eq} [25], Ni_{bal} [30] and $\bar{M}_d$. It is evident from this figure that the $\bar{M}_d$ approach provides a viable estimate of the $\gamma/\sigma + \gamma$ phase boundary in wrought type 316 material. No examples of sigma-free weld metal have been reported.

Fig. A1 also demonstrates that the other methods proposed for the prediction of sigma phase formation, i.e. Cr_{eq} and Ni_{bal}, are less satisfactory in providing a critical value below which sigma phase is not thermodynamically stable. The critical $\bar{M}_d$ value above which sigma phase is in equilibrium with austenite in type 316 material at 600 to 650° C can be estimated from Fig. A1 as 0.906.

References

1. J. K. L. LAI, *J. Nucl. Mater.* **99** (1981) 148.
2. P. RABBE and J. HERITIER, ASTM STP 679 (American Society for Testing and Materials, Philadelphia, 1979) p. 124.
3. C. A. P. HORTON and B. A. SENIOR, Unpublished research.
4. C. J. NOVAK, "Handbook of Stainless Steels", edited by Peckner and Bernstein, (McGraw-Hill, New York, 1977) p. 4–1.
5. S. KIHARA, M. NAKASHIRO, H. UMAKI and J. F. DELONG, in Proceedings First International Conference, Improved Coal-Fired Power Plants, November 19–21, 1986, Palo Alto, California Session 4, Paper 7.
6. R. G. THOMAS, *Welding J.* **58** (1978) 81s.
7. R. A. FARRAR, *J. Mater. Sci.* **22** (1987) 363.
8. *Idem*, "Microstructure and Phase Transformations in Duplex 316 Submerged Arc Weld Metals," MEL Note No. TPRD/M/1251/N82 (1983).
9. W. T. DE LONG, *Welding J.* **53** (1973) 273s.
10. F. H. CHUNG, Proceedings 22 Annual Conference Applied X-ray Analysis, Adv. in X-ray An., "Adv. in X-ray An. Vol. 17", Denver, 22–24 August 1973.
11. J. K. L. LAI and I. F. GALBRAITH, *J. Mater. Sci.* **15** (1980) 1297.
12. B. A. SENIOR, *J. Mater. Sci.* **23** (1988) 2479.
13. L. P. STOTER, *ibid.* **16** (1981) 1039.
14. B. WEISS, C. W. HUGHES and R. STICKLER, *Pract. Metall.* **VIII** (1971) 528.
15. V. P. KUJANPAA, N. J. SUUTALA, T. K. TAKALO and T. J. I. MOISIO, *Metal Constr.* **12** (1980) 282.
16. A. L. SCHAEFFLER, *Metal Prog.* **56** (1949) 680.
17. R. A. FARRAR and R. G. THOMAS, *J. Mater. Sci.* **18** (1983) 3461.
18. J. M. VITEK and S. A. DAVID, *Welding J.* **65** (1986) 106s.
19. M. DEIGHTON., *J. Iron Steel. Inst.* **208** (1970) 1012.
20. D. R. HARRIES, Proceedings International Conference Mechanical Behaviour and Nuclear Applications of Stainless Steels at Elevated Temperature 20-22 May 1981, Varese, Italy, p. 1.
21. W. B. PEARSON, "The Crystal Chemistry and Physics of Metals and Alloys", (Wiley-Interscience, New York, 1972).
22. R. F. DECKER, Proceedings Steel Strengthening Mechanism Symposium, Zurich, Switzerland, (1969) p. 1.
23. M. MORINAGA, N. YUKAWA and H. EZAKI, *Phil. Mag. A* **51** (1985) 223.
24. H. EZAKI, M. MORINAGA, N. YUKAWA and H. ADACHI, *Phil. Mag. A.* **53** (1986) 709.

25. F. C. HULL, *Welding J.* **52** (1973) 104s.
26. M. INAGAKI, T. KASUGAI, K. EI, T. GODAI and O. TANAKA, *Trans. Natl. Res. Inst. Metals* **25** (1983) 121.
27. Y. MINAMI, H. KIMURA and Y. IHARA, *Mater. Sci. Technol.* **2** (1986) 795.
28. C. E. SPAEDER and K. G. BRICKNER, ASTM STP369 (Americal Society for Testing and Materials, Philadelphia, 1965).
29. J. K. L. LAI and A. WICKENS, *Acta Metall.* **27** (1979) 217.
30. J. F. DE LONG, W. F. SIDDALL, F. V. ELLIS, H. HANEDA, T. TSUCHIYA, T. DAIKOKU, F. MASUYAMA and K. SETOGUCHI, Mitsubishi Boiler Bulletin Na MBB-84112E.

Received 15 August 1988
and accepted 14 April 1989